Z. Phys. C – Particles and Fields 9, 177–186 (1988)

Zeitschrift für Physik C Particles and Fields

Hyperon production in e^+e^--annihilation at 10 GeV center of mass energy

ARGUS Collaboration

H. Albrecht, P. Böckmann, R. Gläser, G. Harder, A. Krüger, A. Nippe, M. Schäfer, W. Schmidt-Parzefall, H. Schröder, H.D. Schulz, F. Sefkow, J. Spengler, R. Wurth, A. Yagil
DESY, D-2000 Hamburg, Federal Republic of Germany

R.D. Appuhn, A. Drescher, D. Kamp, H. Kolanoski, U. Matthiesen, H. Scheck, G. Schweda, B. Spaan, A. Walther, D. Wegener
Institut für Physik[1], Universität, D-4600 Dortmund, Federal Republic of Germany

J.C. Gabriel, T. Ruf, K.R. Schubert, J. Stiewe, K. Strahl, R. Waldi, S. Werner
Institut für Hochenergiephysik[2], Universität, D-6900 Heidelberg, Federal Republic of Germany

K.W. Edwards[3], W.R. Frisken[4], D.J. Gilkinson[5], D.M. Gingrich[5], H. Kapitza[3], R. Kutschke[5], D.B. MacFarlane[6], W. McLean[6], A.W. Nilsson[6], R.S. Orr[5], J.A. Parsons[5], P.M. Patel[6], J.D. Prentice[5], J.D. Swain[5], G. Tsipolitis[6], T.-S. Yoon[5]
Institute of Particle Physics[7], Canada

R. Ammar, S. Ball, D. Coppage, R. Davis, S. Kanekal, N. Kwak
University of Kansas[8], Lawrence, KS 66044, USA

B. Boštjančič, G. Kernel, P. Križan
Institute J. Stefan and Oddelek of Physics[9], University of Ljubljana, YU-61000 Ljubljana, Yugoslavia

L. Jönsson
Insitute of Physics[10], University of Lund, S-22362 Lund, Sweden

A. Babaev, M. Danilov, B. Fominykh, A. Golutvin, I. Gorelov, V. Lubimov, V. Matveev, A. Semenov, S. Semenov, V. Shevchenko, V. Soloshenko, V. Tchistilin, I. Tichomirov, Yu. Zaitsev
Institute of Theoretical and Experimental Physics, SU-117259 Moscow, USSR

R. Childers, C.W. Darden, R.C. Fernholz
University of South Carolina[11], Columbia, SC 29208, USA

Received 8 March 1988

[1] Supported by the German Bundesministerium für Forschung und Technologie, under the contract number 054DO51P
[2] Supported by the German Bundesministerium für Forschung und Technologie, under the contract number 054HD24P
[3] Carleton University, Ottawa, Ontario, Canada
[4] York University, Downsview, Ontario, Canada
[5] University of Toronto, Toronto, Ontario, Canada
[6] McGill University, Montreal, Quebec, Canada
[7] Supported by the Natural Sciences and Engineering Research Council, Canada
[8] Supported by the U.S. National Science Foundation
[9] Supported by Raziskovalna skupnost Slovenije and the Internationales Büro KfA, Jülich
[10] Supported by the Swedish Research Council
[11] Supported by the U.S. Department of Energy, under contract DE-AS09-80ER10690

Abstract. The production cross sections for the Λ, Σ^0, Ξ^-, $\Sigma^\pm$ (1385), Ξ^0 (1530) and Ω^- hyperons have been measured, both in the continuum and in direct Υ decays. Baryon rates in direct Υ decays are enhanced by a factor of 2.5 or more compared to the continuum. Such a large baryon enhancement cannot be explained by standard fragmentation models. The strangeness suppression for baryons and mesons turns out to be the same. A strong suppression of spin $\frac{3}{2}$ states is observed.

Introduction

The production of octet and decuplet hyperons in e^+e^--annihilation has been observed recently [1]. These data extend and supplement the information collected on baryon production in other deep inelastic reactions [2–5]. Measurements of hyperon production in direct Υ decays and in the adjacent continuum are of special interest, since a comparison of the respective rates allows for a study of hyperon production in quark and gluon fragmentation. The enhanced baryon rates observed in direct Υ decays [3, 4] might be interpreted as an indication of differences between the fragmentation of quarks and gluons. Precise baryon data are of great importance for settling this problem, particularly since new meson data have been measured recently [6].

In this paper we present a measurement of Λ and Ξ^- momentum spectra in the continuum and in direct decays of the $\Upsilon(1S)$ and $\Upsilon(2S)$. The production rates of Σ^0, $\Sigma^\pm(1385)$, $\Xi^0(1530)$, and Ω^- have been determined separately for the continuum and direct Υ decays. These measurements expand and supplement our recently published results [1], for example through the inclusion of differential cross sections, and due to the appreciably improved statistics for the continuum sample.

Data analysis

The data were collected with the ARGUS detector at the DORIS II storage ring at DESY at center-of-mass energies between 9.4 and 10.6 GeV. The detector, its trigger and particle identification capabilities have been described elsewhere [7]. The event sample used corresponds to an integrated luminosity of 25.7 pb^{-1} on the $\Upsilon(1S)$, 29.3 pb^{-1} on the $\Upsilon(2S)$, 95.4 pb^{-1} on the $\Upsilon(4S)$ and 42.3 pb^{-1} in the continuum. For the study of the low statistics Ω^- and Σ^0 signals the full $\Upsilon(1S)$ data sample of 39.4 pb^{-1} was exploited, although part of it was collected with a reduced magnetic field. Note also that, except for the analysis of the Λ and the Ξ^-, the $\Upsilon(1S)$ and $\Upsilon(2S)$ data have been combined while the $\Upsilon(4S)$ was added to the continuum sample. Hyperon production from B meson decays has been taken into account for the Σ^0 and the $\Sigma^\pm(1385)$, which are expected decay products of the Λ_c. Since the corresponding branching fractions are unknown, it has been assumed that in a $B\bar{B}$ event the rate for Σ-like baryons is half the continuum rate whereas it is zero for hyperons carrying more than one strange quark. The uncertainty in the presented rates for continuum data due to $B\bar{B}$ contributions is estimated to be 13% and is included in the systematic error.

Multihadron events were selected by demanding $\geqq 3$ charged tracks from the main vertex or $\geqq 3$ charged tracks plus an energy deposition of >1.7 GeV in the shower counters. To reduce the background of beam-gas and beam-wall events a cut on a linear combination of the momentum sum of all detected charged and neutral particles and the sum of their momenta along to the beam axis was applied:

$$\sum_i p_i - 1.5 \cdot \left|\sum_i p_{z,i}\right| > 0.25 \cdot \sqrt{s}.$$

This cut efficiently removes contributions to the Λ rate from these background reactions. The efficiency for multihadron events containing a Λ to pass these cuts is 95%, as determined from the data by studying the $\bar{\Lambda}$ signal only, where no background contribution is expected. The remaining background contribution to the Λ rate has been estimated to be less than 1%.

The acceptance of charged tracks was defined by cuts on transverse momentum $p_t > 0.06$ GeV/c and polar angle $|\cos\theta| < 0.92$. For a given charged track all mass hypotheses were accepted for which the likelihood ratio [8] constructed from the combined dE/dx and time-of-flight measurements exceeded 5%. Λ particles were selected by a cut on the χ^2 of the secondary vertex of the $p\pi^-$-combination*. Only protons with a momentum above 0.3 GeV/c were used in the analysis. In addition the Λ candidate had to fulfil the requirement that its polar angle satisfies $|\cos\theta| < 0.85$, and the distance R from the secondary vertex to the beam axis was constrained to lie in the interval $4\text{ cm} < R < 40\text{ cm}$. The opening angle between the p and the π^- was required to satisfy $\cos(p, \pi^-) < 0.998$, in order to reject background from converted photons. To suppress Λ particles from charge-exchange reactions in the inner detector material, the angle between the flight direction of the Λ and the vector $\mathbf{d}$ connecting the main and the secondary vertex had to be $\cos(\mathbf{p}, \mathbf{d}) > 0.995$. Again the remaining background is reduced below 1% after this cut. This cut

* References to specific states are to be interpreted as also implying the charged conjugate state

was not applied to Λ particles used in the search of Ξ^- and Ω^- hyperons, where the Λ does not originate from the main vertex.

For acceptance corrections an overall efficiency was associated with each particle combination. The total acceptance was constructed from a Monte-Carlo detector simulation as a product of two components:

1. $\varepsilon_{\text{comb}}$ reflects the probability for the reconstruction of a selected particle combination. It is given by the product of more fundamental detector acceptances such as the track efficiency, absorption and decay of particles, vertex reconstruction efficiency and losses due to particle identification cuts. Each of these efficiencies is described by a function of one or two properly chosen parameters listed in Table 1.
2. $\varepsilon_{\text{geom}}$ corrects for those combinations having zero acceptance. This includes the geometric acceptance and losses due to kinematical cuts, parametrized as a function of the particle momentum.

An overall weighting factor of

$$w = s \cdot r_c / (\varepsilon_{\text{geom}} \cdot \varepsilon_{\text{comb}})$$

was assigned to each particle combination where s is the center-of-mass energy squared and r_c is a factor representing the radiative corrections for continuum data. This technique has several advantages:

- Acceptance corrections can be performed without relying sensitively on specific distributions in the event generator, e.g. the momentum distribution, if this cannot be measured with enough precision.

Table 1. Parameters used for the acceptance function $\varepsilon_{\text{comb}}$

component	parameter(s)
Track efficiency	p, $\lvert\cos\theta\rvert$
Vertex efficiency	R, $\cos(p, \pi^-)$
Particle absorption	p
Particle identification	p

- The time dependence of acceptances due to new detector components can easily be taken into account.

The systematic error of the factorization ansatz was determined by a Monte-Carlo calculation to be less than 2%. Note that the invariant mass distributions presented are weighted in the described way, normalized by the luminosity to the natural scale of $s \cdot d\sigma/dm$ in units nb·GeV·c^2.

The $p\pi^-$ mass distribution for $x_p > 0.1$ is shown in Fig. 1, where x_p is the scaled momentum $p/p_{\max}$. An almost background-free Λ signal, with a width of 1.6 MeV/c^2, is observed. The Λ cross section was determined by side-band subtraction. Here the mass interval of 1.105–1.125 GeV/c^2 was treated as the signal region, while the intervals of 1.095–1.105 and 1.125–1.135 GeV/c^2 were used as lower and upper side-bands for background subtraction.

Figure 2 shows the $\Lambda\pi^-$ mass distribution for the $\Upsilon(1S)$ and the continuum data. In this decay channel the Ξ^- and the $\Sigma^-(1385)$ resonances are expected. The total momentum of the combination had to exceed $x_p > 0.15$. Only those combinations where a Λ-candidate had a momentum $p > 0.4$ GeV/c and a $\chi^2 < 9$ for the Λ mass hypothesis were considered. A mass constrained fit was applied to the $p\pi^-$-system. A gaussian was used to parametrize the Ξ^- signal, while a 3rd-order polynomial function with a square-root threshold behaviour represents the combinatorial background. In addition a relativistic p-wave Breit-Wigner [9] with fixed mass and width is used to describe the $\Sigma^-(1385)$ resonance. A prominent Ξ^- signal is observed at a mass of 1321.2 ± 0.6 MeV/c^2 and a gaussian width of 4.2 MeV/c^2, while in this plot there is nearly no evidence for the $\Sigma^-(1385)$. The systematic error in determining the Ξ^- signal from this fitting procedure was determined by a Monte-Carlo analysis to be 5%.

In order to analyse the $\Sigma^-(1385)$ signal the pion track, which in the case of the decay $\Sigma^-(1385) \to \Lambda\pi^-$ is prompt, was required to point to the main vertex

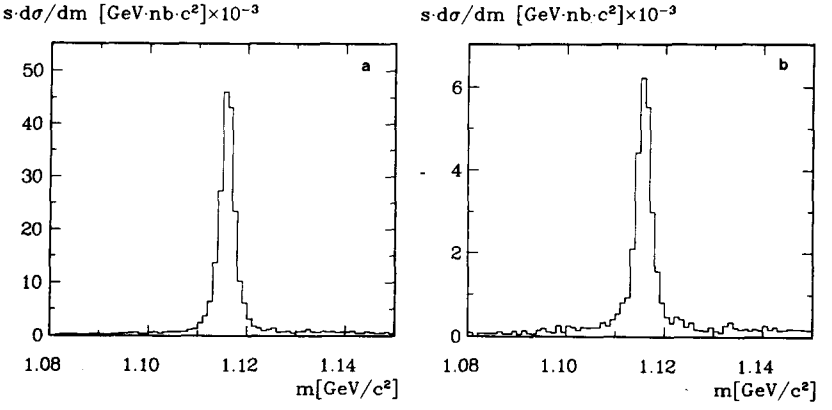

Fig. 1a, b. Mass distributions of $p\pi^-$ combinations with $x_p > 0.1$ **a** for $\Upsilon(1S)$ data, **b** continuum data

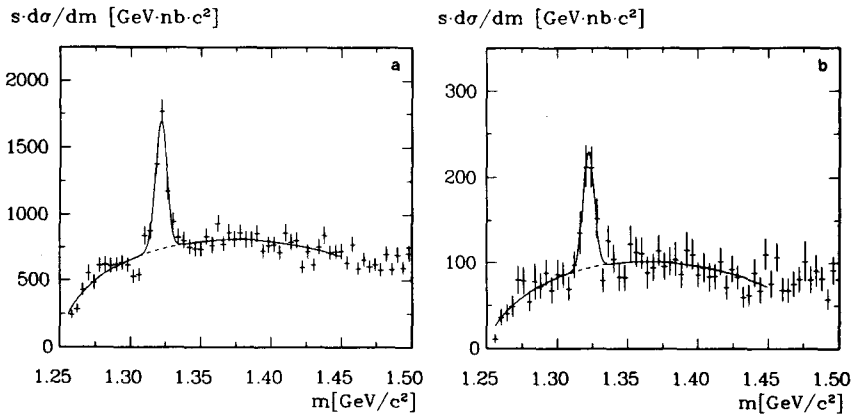

Fig. 2a, b. Mass distributions of $\Lambda\pi^-$ combinations with $x_p > 0.15$ **a** for $\Upsilon(1S)$ data, **b** continuum data

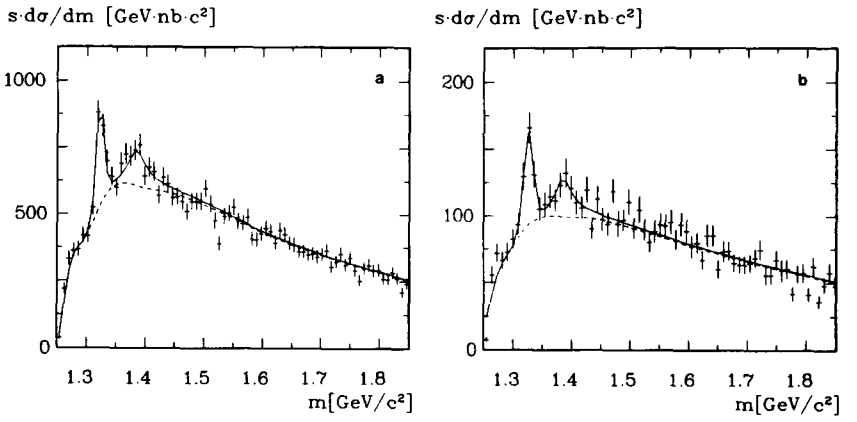

Fig. 3a, b. Mass distributions of combinations with $x_p > 0.15$ of Λ candidates with a prompt π^--track **a** for $\Upsilon(1S)$ and $\Upsilon(2S)$ data, **b** for $\Upsilon(4S)$ and continuum data

region within seven standard deviations. Again a momentum cut of $x_p > 0.15$ was applied. In Fig. 3 the $\Lambda\pi^-$ mass combinations for the combined $\Upsilon(4S)$ and continuum data and the combined $\Upsilon(1S)$ and $\Upsilon(2S)$ data samples are shown. A smoothed Monte-Carlo background, normalized to the data in the mass region between 1.6 and 1.85 GeV/c^2, was used to extract the signal contribution. The signal was integrated within the mass interval of 1.35–1.42 GeV/c^2. The systematic uncertainty on the background normalization was determined by dividing the normalization region into 5 mass intervals. Again, the signal was determined using each of these intervals separately for normalization, which serves as a test of how well the slope of the Monte-Carlo background fits the data. A total systematic uncertainty of 8% was derived by this method. To show that the signal in Fig. 3 has the correct shape, a p-wave Breit-Wigner with fixed mass and width was fitted to the background subtracted mass distribution. The fitted function was then added to the Monte-Carlo background and superimposed to the data points.

A similar analysis was performed for the $\Sigma^+(1385)$ decaying to $\Lambda\pi^+$. The corresponding mass distributions with a momentum cut $x_p > 0.15$ for the Υ and continuum data are shown in Fig. 4. Here an event mixing background resulted in a better description of the data. It can be shown [10] that ΛK^+ correlations, where the K^+ is misidentified as a pion, influence the background distribution. Thus the event mixing was performed only between events with particle (or anti-particle) combinations, in order to take into account for this strangeness correlation. Employing the same error analysis as in the case of the $\Sigma^-(1385)$, the systematic error of the background subtraction was estimated to be 9%.

Ξ^- candidates were obtained by selecting $\Lambda\pi^-$ combinations within a region of ± 10 MeV/c^2 around the Ξ^- mass and with momentum $p > 0.4$ GeV/c. These are combined with an additional π^+ candidate to produce the invariant mass combinations shown in Fig. 5. Again, only combinations with $x_p > 0.15$ were considered. A clear signal at the position of the $\Xi^0(1530)$ is visible in the combined $\Upsilon(1S)$ and $\Upsilon(2S)$ data, while a considerably weaker signal of 3 standard deviations significance is observed in the continuum. The signals were fitted with a p-wave Breit-Wigner of fixed width ($\Gamma = 9.1$ MeV/c^2), folded with a gaussian of free width, while the background was described by a square-root times a 3rd-order polyno-

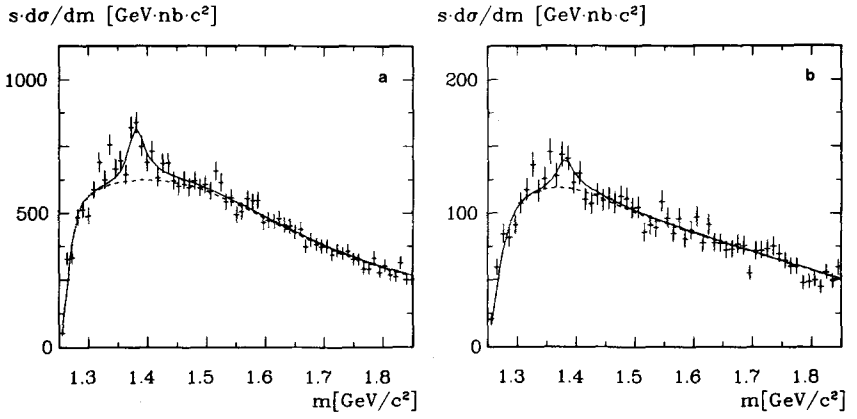

Fig. 4a, b. Mass distributions of combinations with $x_p > 0.15$ of Λ candidates with a prompt π^+-track **a** $\Upsilon(1S)$ and $\Upsilon(2S)$ data **b** for $\Upsilon(4S)$ and continuum data

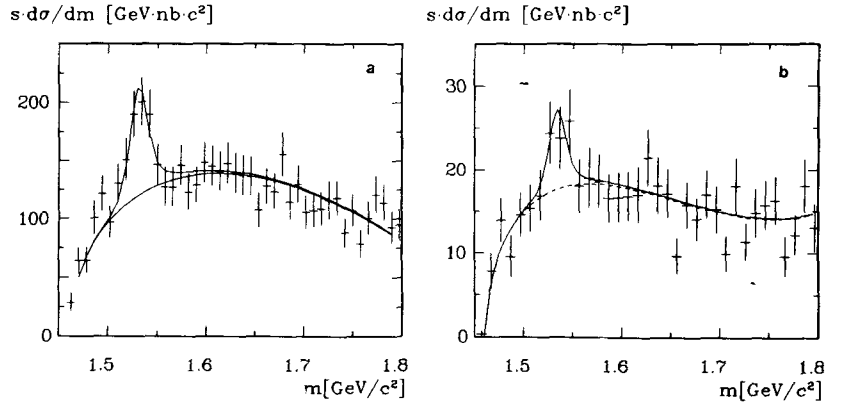

Fig. 5a, b. Mass distributions of combinations with $x_p > 0.15$ of Ξ^- candidates with a prompt π^+-track **a** for $\Upsilon(1S)$ and $\Upsilon(2S)$ data, **b** for $\Upsilon(4S)$ and continuum data

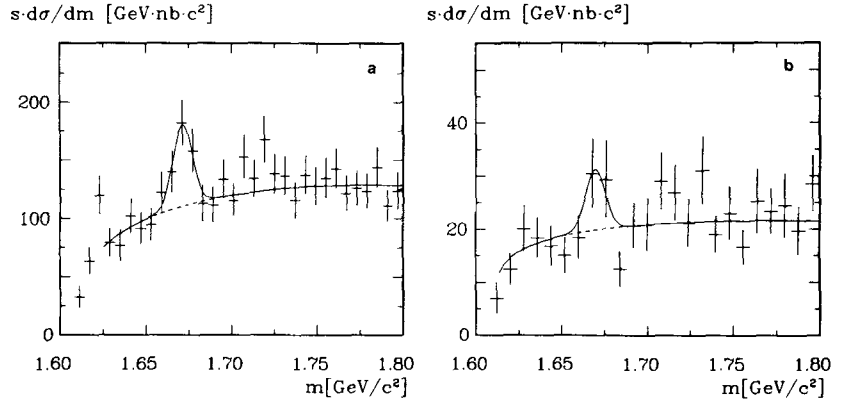

Fig. 6a, b. Mass distributions of ΛK^- combinations with $x_p > 0.15$, **a** for $\Upsilon(1S)$ and $\Upsilon(2S)$ data, **b** for $\Upsilon(4S)$ and continuum data

mial. The fitted mass of the observed resonance is $1530.6 \pm 1.1 (1534.1 \pm 3.8)$ MeV/c^2 for the combined Υ (continuum) data. A gaussian width of 6.5 MeV/c^2 was obtained from the fit to the Υ data, which is compatible with the detector resolution. The width was fixed to this value when fitting the continuum data.

The ΛK^- invariant mass distributions with $x_p > 0.15$ are plotted in Fig. 6. A clear Ω^- signal is observed in the Υ data, while in the continuum sample an enhancement with only a marginal significance is visible. The invariant mass distribution was fitted with a square-root times 3rd-order polynomial plus a gaussian of free mass and width in case of the Υ data. The region between 1.75–1.85 GeV/c^2 was left out of the fit since contributions from the Ξ^- reflection due to π/K misidentification are expected there. The mass and width determined from this fit are $m = 1671.2 \pm 1.1$ MeV/c^2 and $\sigma = 5.7 \pm 1.1$ MeV/c^2. By fitting the continuum sample, a small positive signal

at a mass of 1669.6 ± 5.5 MeV/c^2 was obtained, using a width fixed to the value given above.

Finally in Fig. 7 we show the invariant mass of $\Lambda\gamma$ combinations, where the photon has converted into an e^+e^--pair forming a secondary vertex [11]. Note that all data have been combined to achieve this signal. The excellent energy resolution for converted photons results in a narrow signal with $m = 1193.4 \pm 0.7$ MeV/c^2 and $\sigma = 2.3 \pm 0.6$ MeV/c^2. A 3rd-order polynomial plus a gaussian was used to describe the invariant mass distribution.

The acceptance corrected rates were divided by the corresponding branching ratios, taken from [12], for each specific channel and for the decay $\Lambda \to p\pi^-$. For broad resonances an additional correction for the tail of the mass distribution was applied, integrating the Breit-Wigner function numerically up to 2.5Γ. The extrapolation to the unobserved momentum range was done for the Λ and Ξ^- particles by fitting a function

$$\frac{1}{\beta\sigma_{\text{had}}} \cdot \frac{d\sigma}{dz} = A \cdot \exp(-b \cdot z)$$

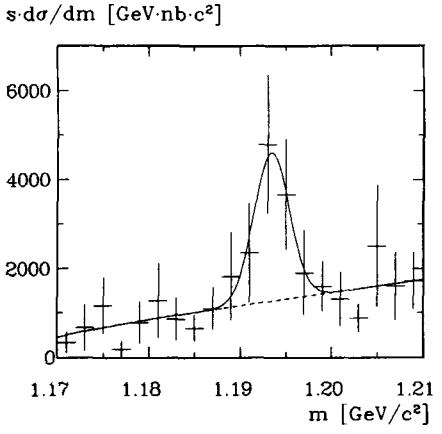

Fig. 7. Mass distributions of $\Lambda\gamma_c$ combinations with $x_p > 0.15$, where γ_c is a converted photon. All available data have been combined for this plot

with $z = 2 \cdot E/\sqrt{s}$ to the particle spectrum, where E is the hyperon energy. For all other resonances the shape of the Ξ^- spectrum was used for extrapolation. The Ξ^- spectrum was used instead of the Λ spectrum since our data show that Λ particles are to a high degree decay products of heavier hyperons, and hence their spectrum is slightly softened. A momentum cut of $x_p > 0.15$ retains 78.7% of the events in Υ decays and 82% in the continuum. The results of particle rates per event are collected in Table 2. The first error given is purely statistical, while the second includes the systematic errors of the acceptance correlation, the analysing procedure, the multihadron selection and the momentum extrapolation.

Discussion of results and comparison with model predictions

The Λ spectra $1/\sigma_{\text{had}} \cdot d\sigma/dx_p$ for $\Upsilon(1S)$, $\Upsilon(2S)$ and continuum are shown in Fig. 8a and, for further illustration, listed in Table 3. In addition, the Λ continuum spectrum $1/\beta\sigma_{\text{had}} \cdot d\sigma/dz$ has been included in Table 4. Note that QED radiative corrections have been applied to the continuum data. The particle spectra for direct $\Upsilon(1S)$ and $\Upsilon(2S)$ decays are obtained from the measured distributions at the resonance energies by subtracting the contributions from the continuum and the vacuum polarisation. As demonstrated in Fig. 8a, the direct $\Upsilon(1S)$ and $\Upsilon(2S)$ spectra are, within errors, identical. A comparison of the Λ spectra from continuum and direct $\Upsilon(1S)$ decays demonstrates that the former are harder. The predictions of the LUND string model (version 6.2) [14] are included in the figure. In case of the $\Upsilon(1S)$ data the shape of the spectra is reproduced approximately, but the absolute Λ rate turns out to be appreciably larger than predicted by the model. The measured continuum spectrum for Λ particles deviates from the model predictions, particularly at large momenta where the model predicts a higher rate.

The spectra of Ξ^- hyperons from continuum fragmentation and direct $\Upsilon(1S)$ decays are compared in

Table 2. Hyperon rates per multihadronic event in direct Υ decays and in the continuum

baryon	Υ^{dir}	continuum
Λ	$(2.28 \pm 0.03 \pm 0.21) \times 10^{-1}$	$(0.92 \pm 0.03 \pm 0.08) \times 10^{-1}$
Ξ^-	$(2.06 \pm 0.17 \pm 0.23) \times 10^{-2}$	$(0.67 \pm 0.06 \pm 0.07) \times 10^{-2}$
Σ^{0a}	$(5.64 \pm 1.69 \pm 1.13) \times 10^{-2}$	$(2.29 \pm 0.69 \pm 0.49) \times 10^{-2}$
$\Sigma^-(1385)$	$(1.42 \pm 0.17 \pm 0.20) \times 10^{-2}$	$(0.553 \pm 0.109 \pm 0.098) \times 10^{-2}$
$\Sigma^+(1385)$	$(1.68 \pm 0.29 \pm 0.23) \times 10^{-2}$	$(0.513 \pm 0.095 \pm 0.092) \times 10^{-2}$
$\Xi^0(1530)$	$(4.78 \pm 1.14 \pm 0.62) \times 10^{-3}$	$(1.46 \pm 0.51 \pm 0.23) \times 10^{-3}$
Ω^-	$(1.83 \pm 0.62 \pm 0.32) \times 10^{-3}$	$(0.72 \pm 0.36 \pm 0.13) \times 10^{-3}$

[a] The Σ^0 rate was separated between direct Υ decays and continuum by using the r value of the Λ

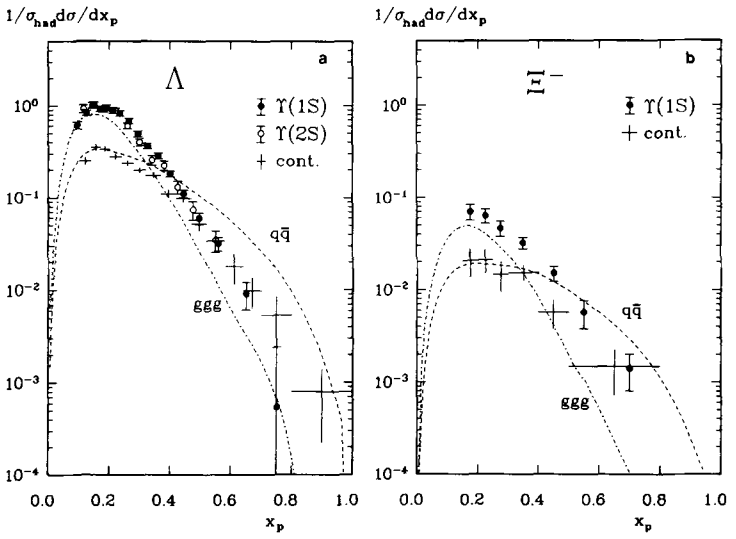

Fig. 8a, b. Inclusive spectra $1/\sigma_{had} \cdot d\sigma/dx_p$ for direct Υ and continuum data as a function of the scaled momentum x_p. The dashed and dash-dotted curves show the predictions of the LUND model **a** for Λ hyperons, **b** for Ξ^- hyperons

Table 3a. Λ spectrum $\frac{1}{\sigma_{had}} \frac{d\sigma}{dx_p}$ for $\Upsilon(1S)$ direct decays

x_p interval	cross section	x_p internal	cross section
0.08–0.11	$0.606 \pm 0.059 \pm 0.053$	0.31–0.34	$0.360 \pm 0.020 \pm 0.031$
0.11–0.14	$0.835 \pm 0.047 \pm 0.073$	0.34–0.38	$0.283 \pm 0.016 \pm 0.025$
0.14–0.16	$1.026 \pm 0.055 \pm 0.089$	0.38–0.42	$0.181 \pm 0.014 \pm 0.016$
0.16–0.18	$0.919 \pm 0.048 \pm 0.080$	0.42–0.47	$0.110 \pm 0.011 \pm 0.010$
0.18–0.20	$0.947 \pm 0.046 \pm 0.082$	0.47–0.52	$0.060 \pm 0.009 \pm 0.005$
0.20–0.22	$0.890 \pm 0.042 \pm 0.077$	0.52–0.60	$0.032 \pm 0.005 \pm 0.003$
0.22–0.25	$0.823 \pm 0.031 \pm 0.072$	0.60–0.70	$0.009 \pm 0.003 \pm 0.001$
0.25–0.28	$0.680 \pm 0.027 \pm 0.059$	0.70–0.80	0.001 ± 0.001
0.28–0.31	$0.491 \pm 0.023 \pm 0.042$	0.80–1.00	–

Table 3b. Λ spectrum $\frac{1}{\sigma_{had}} \frac{d\sigma}{dx_p}$ for $\Upsilon(2S)$ direct decays

x_p interval	cross section	x_p interval	cross section
0.10–0.13	$0.927 \pm 0.090 \pm 0.079$	0.32–0.36	$0.254 \pm 0.030 \pm 0.022$
0.13–0.16	$1.014 \pm 0.076 \pm 0.086$	0.36–0.40	$0.222 \pm 0.027 \pm 0.019$
0.16–0.20	$0.909 \pm 0.054 \pm 0.077$	0.40–0.45	$0.130 \pm 0.021 \pm 0.011$
0.20–0.24	$0.878 \pm 0.047 \pm 0.075$	0.45–0.50	$0.074 \pm 0.017 \pm 0.006$
0.24–0.28	$0.600 \pm 0.039 \pm 0.051$	0.50–0.60	$0.034 \pm 0.009 \pm 0.003$
0.28–0.32	$0.401 \pm 0.033 \pm 0.034$	–	–

Table 3c. Λ spectrum $\frac{1}{\sigma_{had}} \frac{d\sigma}{dx_p}$ for continuum data

x_p interval	cross section	x_p interval	cross section
0.10–0.14	$0.248 \pm 0.025 \pm 0.021$	0.42–0.47	$0.098 \pm 0.010 \pm 0.008$
0.14–0.17	$0.348 \pm 0.028 \pm 0.030$	0.47–0.52	$0.052 \pm 0.008 \pm 0.004$
0.17–0.20	$0.333 \pm 0.024 \pm 0.028$	0.52–0.58	$0.034 \pm 0.007 \pm 0.003$
0.20–0.24	$0.275 \pm 0.019 \pm 0.029$	0.58–0.64	$0.018 \pm 0.006 \pm 0.002$
0.24–0.28	$0.236 \pm 0.016 \pm 0.020$	0.64–0.70	$0.010 \pm 0.004 \pm 0.001$
0.28–0.32	$0.198 \pm 0.014 \pm 0.017$	0.70–0.80	0.005 ± 0.003
0.32–0.37	$0.173 \pm 0.013 \pm 0.015$	0.80–1.00	0.001 ± 0.001
0.37–0.42	$0.109 \pm 0.011 \pm 0.009$	–	–

Table 4. Λ spectrum $\frac{1}{\beta\sigma_{\text{had}}}\frac{d\sigma}{dz}$ for continuum data

z interval	cross section	z interval	cross section
0.23–0.25	$1.190\pm0.144\pm0.095$	0.38–0.42	$0.259\pm0.021\pm0.021$
0.25–0.26	$1.109\pm0.140\pm0.089$	0.42–0.46	$0.145\pm0.018\pm0.012$
0.26–0.27	$1.044\pm0.121\pm0.083$	0.46–0.50	$0.108\pm0.015\pm0.009$
0.27–0.28	$0.785\pm0.096\pm0.063$	0.50–0.55	$0.064\pm0.011\pm0.005$
0.28–0.29	$0.781\pm0.089\pm0.063$	0.55–0.60	$0.055\pm0.010\pm0.004$
0.29–0.30	$0.628\pm0.078\pm0.050$	0.60–0.70	$0.016\pm0.005\pm0.001$
0.30–0.32	$0.496\pm0.044\pm0.040$	0.70–0.80	$0.008\pm0.003\pm0.001$
0.32–0.34	$0.398\pm0.038\pm0.032$	0.80–1.00	0.003 ± 0.001
0.34–0.38	$0.301\pm0.022\pm0.024$	–	–

Fig. 8b. The data points are listed in Tables 5 and 6. Again, the continuum data have the harder spectrum and the predictions of the LUND model deviate from the observed distributions. Both the Λ and the Ξ^- spectra are consistent with those measured by the CLEO collaboration [4] at comparable energies.

From the particle rates per event collected in Table 2 it follows that the production rate of all hyperons is much larger in direct Υ decays than in the continuum. To illustrate this in more detail we present in Fig. 9 a plot of the resonance enhancement factor defined as

$$r=\frac{\#\text{ hadrons/event in }\Upsilon(1S)\text{ decays}}{\#\text{ hadrons/event in the continuum}}.$$

Besides the presented results we have included results taken from [6, 13]. This figure demonstrates that the baryon enhancement in Υ decays is not a mass effect, as predicted by colour singlet cluster models [15], since heavy mesons, as the η and ϕ, show no such enhancement.

It should be pointed out that also the LUND string model cannot reproduce the measured enhancement factor of $r\simeq 2.5$–3.5. Note, however, that the LUND string model underestimates the Λ production in direct Υ decays and overestimates the rate for continuum events. The origin of the baryon enhancement in the LUND framework is a generally higher particle multiplicity and the possibility of producing diquarks in the first break-up of the closed string in 3 gluon events. Since about 40% of the continuum events are $c\bar{c}$-jets, baryon production in the continuum is further reduced by phase space.

In the LUND model a baryon enhancement of about 2 can be explained with these arguments. There is no other way for this model to produce a substantial baryon enhancement in Υ decay, because the only adjustable parameter influencing the baryon rate is the diquark probability qq/q, which is equal in 3 gluon and $q\bar{q}$ events since in both cases colour triplet strings are assumed to be stretched. Hence the present data indicate that gluons and quarks might fragment differently. Contributions of octet strings to 3 gluon fragmentation [16], a source not considered up to now in the LUND version of the string model, might be a possible explanation for the differences.

Table 5a. Ξ^- spectrum $\frac{1}{\sigma_{\text{had}}}\frac{d\sigma}{dx_p}$ for $\Upsilon(1S)$ direct decays

x_p interval	cross section
0.15–0.20	$0.070\pm0.014\pm0.008$
0.20–0.25	$0.064\pm0.011\pm0.007$
0.25–0.30	$0.047\pm0.009\pm0.005$
0.30–0.40	$0.032\pm0.005\pm0.003$
0.40–0.50	$0.015\pm0.003\pm0.002$
0.50–0.60	$0.006\pm0.002\pm0.001$
0.60–0.80	0.001 ± 0.001

Table 5b. Ξ^- spectrum $\frac{1}{\sigma_{\text{had}}}\frac{d\sigma}{dx_p}$ for continuum data

x_p interval	cross section
0.15–0.20	$0.021\pm0.007\pm0.003$
0.20–0.25	$0.021\pm0.006\pm0.003$
0.25–0.30	$0.015\pm0.005\pm0.002$
0.30–0.40	$0.015\pm0.003\pm0.002$
0.40–0.50	$0.006\pm0.002\pm0.001$
0.50–0.80	0.001 ± 0.001

Table 6. Ξ^- spectrum $\frac{1}{\beta\sigma_{\text{had}}}\frac{d\sigma}{dz}$ for continuum data

z interval	cross section
0.29–0.32	$0.067\pm0.023\pm0.007$
0.32–0.35	$0.049\pm0.014\pm0.005$
0.35–0.39	$0.028\pm0.008\pm0.003$
0.39–0.47	$0.024\pm0.005\pm0.003$
0.47–0.55	$0.008\pm0.003\pm0.001$
0.55–0.83	0.002 ± 0.001

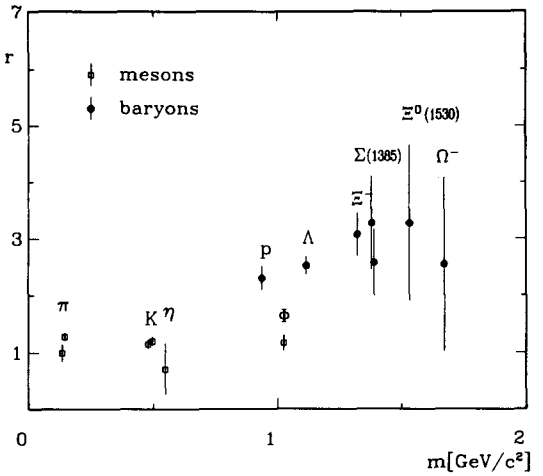

Fig. 9. Ratio r of hadron production rates. The errors given in this plot are statistical only. The meson and proton rates are taken from unpublished ARGUS results [6, 13]

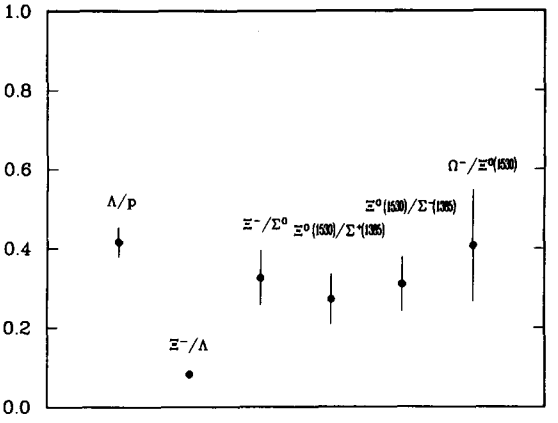

Fig. 10. Strangeness suppression determined from the hyperon production rates. The errors given in this plot are statistical only

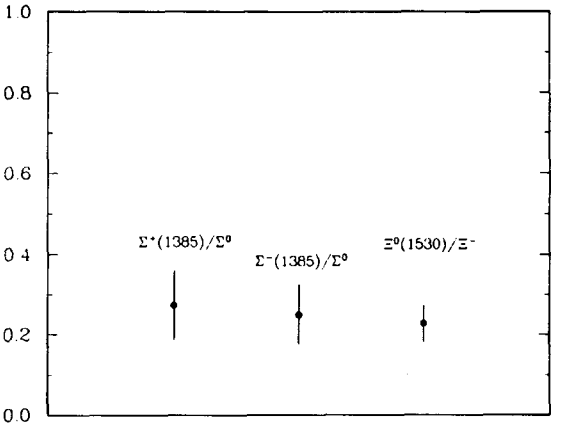

Fig. 11. Spin 3/2 suppression determined from different hyperon production rates. The errors given in this plot are statistical only

It should be stressed that an enhancement of this magnitude has been predicted in [17] in the framework of a cascade multiplication in quark and gluon jets. The free parameters of this model are derived from an analysis of J/ψ decays.

A more straightforward explanation discussed in detail in [10] is based on the assumption, that baryons only to small extent are leading particles in quark jets. This interpretation follows from the observed differences between the measured hyperon spectra shown in Fig. 8a and b and the model predictions at large z. Even stronger evidence for this hypothesis follows from the comparison of the $\Sigma^+(1385)$ and $\Sigma^-(1385)$ production rates in the continuum. Since u-quarks are produced four times more often than d-quarks as primary quarks in e^+e^--annihilation, one would expect a ratio $\Sigma^+(1385)/\Sigma^-(1385)>1$ in $q\bar{q}$ events. Within our present errors the rates of $\Sigma^+(1385)$ and $\Sigma^-(1385)$ are equal, while e.g. the LUND model (version 6.2) predicts a ratio of 1.8. The difference again can be traced back to the suppression of leading baryons in quark jets.

In Fig. 10 the strangeness suppression in baryon production is determined by the production ratio of hyperons which differ by one unit in strangeness. The results from 3 gluon decay and continuum data have been averaged, since they are equal within the present errors. As can be seen, the strangeness suppression is about 0.3 and, within the uncertainty of the measurements, independent of the baryon spin. Thus, the level of strangeness suppression is comparable to the value derived from meson production [18]. This is not generally expected in diquark models, which usually claim that the production of diquarks carrying strangeness and/or spin 1 is suppressed. The most natural explanation of this observation is that the three quarks forming a baryon are produced independently during the fragmentation process [19]. Note that the low Ξ^-/Λ ratio can be explained by the high feed-down from hyperon decays. Adding up the hyperon rates given in Table 2, it follows that feed-down accounts for more than 60% of the total observed Λ rate. Taking the Σ^0 rate as an approximate measure of the direct Λ rate, the strangeness suppression is given by the ratio $\Xi^-/\Sigma^0=0.33\pm0.07\pm0.06$.

Another symmetry breaking effect in the fragmentation process can be studied by comparing the production of octet and decuplet baryons with the same flavour content. Figure 11 shows the spin suppression for the ratios $\Sigma^\pm(1385)/\Sigma^0$ and $\Xi^0(1530)/\Xi^-$. No corrections for feed-down from excited states or for spin statistics have been applied. Nevertheless a strong spin suppression of 0.2–0.3 is observed, far beyond the predictions of colour singlet cluster models [15],

which assume hadron production rates are proportional to spin statistics. Moreover, spin suppression in baryon production cannot be explained by phase space arguments as in meson production, since the mass difference between octet and decuplet baryons is rather small. Therefore, this observation reveals a dynamical aspect of the fragmentation process.

Summary

In a high statistics sample of e^+e^- annihilation data, fragmentation into hyperons has been studied both for continuum events and direct Υ decays. The momentum spectra of the continuum data are harder than those of direct Υ decays. This observation agrees with expectations. The production rate of hyperons is enhanced by a factor of 2.5 or more in direct $\Upsilon(1S)$ decays compared to the continuum. This enhancement is larger than predicted by standard fragmentation models. Tuning of model parameters cannot solve this discrepancy. Hence this observation might indicate inherent differences of quark and gluon fragmentation

The strangeness suppression determined from hyperon production rates turns out to be the same as for meson production. This observation favours fragmentation models which allow for baryon production from independently produced quarks. Baryons with spin $\frac{1}{2}$ are produced more abundantly than those with spin $\frac{3}{2}$. Finally the comparison of $\Sigma^{\pm}(1385)$ production in the continuum leads to the conclusion that baryons are not dominantly leading particles of quark jets.

Acknowledgements. It is a pleasure to thank U. Djuanda, E. Konrad, E. Michel, and W. Reinsch for their competent technical help in running the experiment and processing the data. We thank Dr. H. Nesemann, B. Sarau, and the DORIS group for the excellent operation of the storage ring. The visiting groups wish to thank the DESY directorate for the support and kind hospitality extended to them.

References

1. H. Albrecht et al. ARGUS Collab.: Phys. Lett. 183B (1987) 419
2. R. Brandelik et al. DASP Collab.: Nucl. Phys. B148 (1979) 189; R. Brandelik et al. TASSO: Phys. Lett. 94B (1980) 444; M. Althoff et al. TASSO: Z. Phys. C – Particles and Fields 17 (1982) 5
3. H. Albrecht et al. DASP II Collab.: Phys. Lett. 102B (1981) 291; M.S. Alam et al. CLEO Collab.: Phys. Rev. Lett. 53 (1985) 24
4. S. Behrends et al. CLEO Collab.: Phys. Rev. D31 (1985) 2161
5. W. Bartel et al. JADE Collab.: Phys. Lett. 104B (1981) 325; R. Brandelik et al. TASSO Collab.: Phys. Lett. 105B (1981) 75; S.R. Klein et al. MARK II Collab.: Phys. Rev. Lett. 58 (1987) 644
6. A. Drescher: Thesis, Univ. Dortmund 1987; U. Matthiesen: Thesis, Univ. Dortmund 1987; S. Werner: Diplomarbeit, Univ. Heidelberg 1987, IHEP-HD/87-1
7. H. Albrecht et al. ARGUS Collab.: Phys. Lett. 134B (1984) 137
8. H. Albrecht et al. ARGUS Collab.: Phys. Lett. 150B (1985) 235
9. J.D. Jackson: Nuov. Cimento 34 (1964) 1644
10. H. Scheck: Thesis, Univ. Dortmund 1988
11. A. Philipp: Thesis, Univ. Dortmund 1987
12. Particle Data Group: Phys. Lett. 170B (1986)
13. H. Albrecht et al.: Contributed paper to the XXXIInd International Conference on High Energy Physics, Leipzig 1984
14. B. Andersson et al.: Phys. Rep. 97 (1983) 31
15. R.D. Field: Phys. Lett. 135B (1984) 203
16. I. Montvay: Phys. Lett. 84B (1979) 331
17. Y. I. Azimov et al.: Yad. Fiz. 37 (1983) 703
18. D.H. Saxon: RAC-86-057; A. Wroblewski: Acta Phys. Pol. B16 (1985) 379
19. A. Casher et al.: Phys. Rev. D20 (1979) 179